Graphene Oxide Reinforced Gelatin-poly(vinyl alcohol) Porous Composites for Biomedical Applications

NICOLAE VLADIMIR VOICU[1], LIVIA ELENA CRICA[1], ANDREEA MADALINA PANDELE[1], CELINA MARIA DAMIAN[1]*, EUGENIA VASILE[2], MARIANA IONITA[1]

[1], University Politehnica of Bucharest, Advanced Polymer Materials Group, 1-7 Gh. Polizu Str., 011061, Bucharest, Romania

[2] University Politehnica of Bucharest, 1-7 Gh. Polizu Str., 011061, Bucharest, Romania

This study reports the preparation of gelatin – poly(vinyl alcohol) / graphene oxide composites by combining ultrasound treatment, freeze-thawing and freeze drying techniques. Characterization results highlight the positive effect of graphene oxide on materials structure, morphology, swelling degree and biodegradation, as well as rheology.

Keywords: poly(vinyl alcohol), ultrasound treatment, graphene oxide

Tissue engineering aims to overcome the major problems associated with conventional surgical procedures (autografts and allografts) for tissue reconstruction [1, 2]. Autografts are currently the most suitable solution since they integrate reliably with host tissue and do not trigger inflammatory responses [3]. However, the anatomical limitations and donor site morbidity associated with this technique demand for the development of tissue engineered constructs that will mimic the extracellular matrix (ECM) environment [3, 4].

The key components of synthetic tissue constructs are the cells, the growth-stimulating signals and the scaffolds which act as templates for tissue formation by allowing cells to migrate, adhere, and produce new tissue [5, 6].

In order to sustain cell migration, attachment, proliferation and differentiation scaffolds should exhibit optimal characteristics like good biocompatibility, interconnected pore structure as well as adequate biodegradability and mechanical strength [7]. Moreover, biodegradation of the scaffold should take place with the same rate as the rate of new tissue regeneration in order to maintain a good structural integrity of the healing site [8, 9]. In this context, it is essential to choose appropriate materials and couple them with suitable fabrication techniques in order to satisfy the criteria listed above.

Biopolymer-based materials that resemble the extracellular matrix (ECM), like collagen or gelatin, are promising candidates for tissue regeneration since they are degradable under physiological conditions and they represent a recognized substrate for cells enhancing their adhesion and differentiation [10]. Gelatin (Gel) is a natural biopolymer obtained by denaturation of collagen, the most abundant protein in human body [11]. Gelatin has been shown to have several advantages over its parent protein like better solubility in water, a lower level of immunogenicity, and it stimulates angiogenesis [12]. Due to its water solubility and low mechanical strength gelatin needs to be crosslinked and reinforced [13]. Since chemical crosslinked structures have caused tissue inflammation and calcification, gelatin is often combined with synthetic polymers to improve its mechanical properties, control the degradation rate and microstructure [14]. Among biodegradable and biocompatible polymers, polyvinyl alcohol (PVA) is one of the most commonly used polymers for biomedical applications since it is non-toxic, water soluble and possess good mechanical properties [15, 16]. PVA can be physically crosslinked through repeated freeze-thawing cycles avoiding the use of toxic crosslinking agents [17]. The first attempt of PVA crosslinking through freeze-thawing method was reported by Peppas [18]. The mechanism is based on the partial alignment of macromolecular chains during repeated freeze-thawing cycles, resulting in small crystallites that act as physical crosslink junctions [19]. Liu et al. synthesized physically crosslinked PVA/gelatin hydrogels and reported that the hydrogels treated with three freeze-thawing cycles present higher glass transition and melting temperatures, enhanced crystallinity degree as well as higher ultimate strength in comparison to the ones treated with only one freeze-thawing cycle [20].

Conversely, since its discovery in 2004, graphene (G) has gained a lot of attention among the scientific community due to its unique 2D structure that exhibits remarkable mechanical strength as well as high electrical and thermal conductivity [21]. Yet, pristine G is difficult to be exfoliated and distributed homogeneously inside polymer matrixes due to the high interaction forces between graphene sheets [22, 23]. Graphene oxide (GO), on the other hand, possess multiple active polar groups on its surface like carbonyl, hydroxyl and epoxide which makes it readily dispersible in aqueous solutions and facilitates covalent, as well as non-covalent intermolecular interactions with polymer materials [24, 25]. Conversely, GO has been proved to be an excellent reinforcing agent, Lu et al. reported a 132% increase in tensile strength and a 36% improvement of compressive strength with the addition of only 0.8 wt% GO within PVA hydrogels [26]. Moreover, besides the ability to enhance mechanical properties, it was proven that GO sustains and even promotes cell proliferation when used as reinforcing agent for polymer matrices [27], thus, making it an appealing nanofiller for composite materials designed for biomedical applications.

In this paper, we report the fabrication of porous composites based on incorporation of GO as reinforcing agent in Gel-PVA polymer blend. The composite materials having different GO concentrations were treated with 3 freeze-thawing cycles and the final 3D porous structure was obtained by freeze-drying. The synthesized materials were characterized by Fourier Transform Infrared

* *Phone: (+40)214029100*

Spectrometry (FT-IR), Raman Spectrometry and Scanning Electron Microscopy (SEM). Furthermore the swelling behavior, degradation rate and rheological features were investigated.

Experimental part

Materials and Methods

Graphene oxide prepared according to Hummers method [28] was purchased from the National Institute for Research and Development in Microtechnology (Romania). Solid BioReagent Gelatin from cold water fish skin (60 kDa MW), 99% hydrolyzed poly(vinyl alcohol) having an average molecular weight of 130 000 g/mol and P-5368 phosphate buffer saline (PBS) 0.01M were purchased from Sigma Aldrich. Materials were used without further modifications.

Gel-PVA/GO scaffold preparation

Porous scaffolds based on Gel-PVA/GO having the GO weight fractions (wt.) 0.5, 1, 2 and 3 % as well as a GO-free polymer matrix were prepared using a freeze-drying process. Firstly, exfoliation of GO was obtained through ultrasonication in 25 mL deionized water for 1 h. Then, gelatin granules were added under continuous stirring at a temperature of 60 °C until a concentration of 5 wt. % was reached. The PVA solution (5 wt. %) was prepared by dissolving the powder in distilled water at 120 °C in an autoclave and, afterwards, 25 mL were blended with the Gel-GO mixture through a ultrasound treatment for 30 min. Finally, the composite solutions were subjected to 3 cycles of freeze-thawing by freezing 21 h at -70 °C and defrosting 3 h at room temperature. The final 3D structure of porous Gel-PVA/GO composites was obtained by freeze-drying for 100 h.

Equipment employed during scaffold preparation

The ultrasound treatment was done on a VCX750 Sonics & Materials apparatus with a net power output of 750 Watts and a frequency of 20 kHz. The ultrasonic processor was equipped with a titanium alloy (Ti-6Al-4V) probe tip and was operated at an amplitude of 80%. During ultrasonication the temperature of the samples was maintained low using an ice bath in order to avoid local overheating and sample thermal degradation.

Sample freeze-drying was attained using a Crist LCG Alpha 2-4 LD plus lyophilizer equipped with a polymethyl methacrylate (PMMA) chamber. The freeze-drying process parameters were set at a temperature of – 50 °C and 0.040 mbar vacuum for 100 hours.

FT-IR spectrometry

A Bruker Vertex 70 FT-IR spectrometer operated in attenuated total reflection (ATR) mode was used during the measurements of all samples. All spectra were recorded in absorbance mode within a wavenumber range of 600-4000 cm^{-1} at a 4 cm^{-1} resolution with 32 scans per sample.

Raman spectrometry

Raman spectra of synthesized scaffolds were collected by employing a Raman DXR Thermo Scientific instrument with a 532 nm wavelength laser and 3 mW power. The collected data were recorded within a wavenumber range of 50-3500 cm^{-1} by using a 10x objective lense.

Scanning electron microscopy

Morphological studies were performed on a QUANTA INSPECT F scanning electron microscope (SEM) equipped with field emission gun (1.2 nm resolution) and energy dispersive x-ray spectrometer (133 eV, Mn Kα radiation). In order to prevent the accumulation of static electric fields at the specimen and to increase the secondary electron signal, the samples were previously sputter-coated with a thin layer of gold (Au).

Swelling behavior

The aqueous fluid uptake capacity of synthesized scaffolds was determined by means of swelling experiments. The dried scaffolds were immersed in 6 mL of phosphate buffer solution (PBS, *p*H 7.4) at room temperature. The swollen samples were weighted at definite time intervals after wiping off the excess water with filter paper. The swelling degree was determined using equation 1.

$$SWD = \frac{M_t - M_d}{M_d} \cdot 100 \quad (1)$$

where M_t was the total weight of the swollen sample at time *t* and M_d was the dry weight of the scaffold before immersion.

In addition, the equilibrium water content (EWC) of the scaffolds was determined using equation 2.

$$EWC\% = \frac{M_t - M_d}{M_t} \cdot 100 \quad (2)$$

Scaffold degradation

Scaffold degradation was carried out by incubating samples in a *p*H 7.4 phosphate buffer solution (PBS 0.01M) containing 0.05 wt% sodium azide at 37°C. Sodium azide was included in the solution in order to inhibit potential microorganisms and bacteria growth. At different time intervals (3, 15, 45 and 90 days), the samples were removed from PBS and dried in open atmosphere at room temperature until constant weight was reached. The degradation percent was calculated using the equation 3:

$$Deg = \left(1 - \frac{m_0}{m_f}\right) \cdot 100 \quad (3)$$

where m_0 is the initial weight of the scaffold and m_f represents the final weight.

Rheological behaviour

Rheological properties were determined by using a Malvern Kinexus Pro$^+$ rotational rheometer equipped with a 20 mm parallel plate geometry.

Scaffolds were swollen for 1 h in distilled water having the temperature of 37°C and were cut in cylinders with a diameter of 20 mm. Next the samples were loaded and the superior plate was lowered until a normal force of 0.2 N was reached.

Storage modulus (G2) and loss modulus (G3) of the nanocomposite samples were measured as a function of frequency (10^{-1}–10^{1} Hz) using oscillatory tests. In order to perform the frequency sweep tests, the linear viscoelastic range of the samples (LVE) was obtained from amplitude sweep tests (with a stress amplitude between 0.1 and 50 Pa) using a constant frequency ν = 1 Hz.

Results and discussions

FT-IR spectrometry

The gelatin spectrum (fig. 1) presents the characteristic signals of the protein spectra: amides I, II and III together with Amide A [29]. The low intensity Amide A absorption band at 3300 cm^{-1} is represented by the N-H stretching vibration of the peptide bond. The most intense absorption band is the Amide I found at 1650 cm^{-1} generated by the

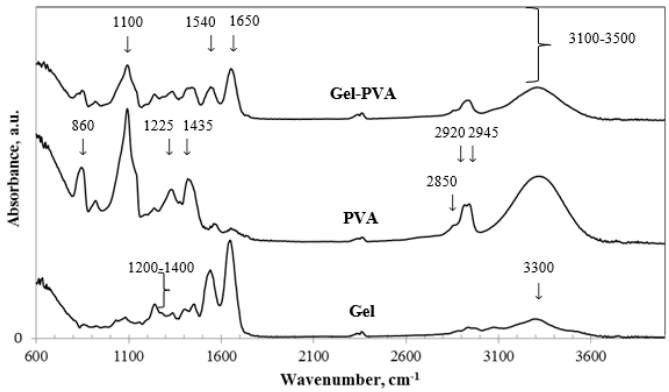

Fig. 1. FT-IR spectra of Gelatin, PVA and the respective polymer blend

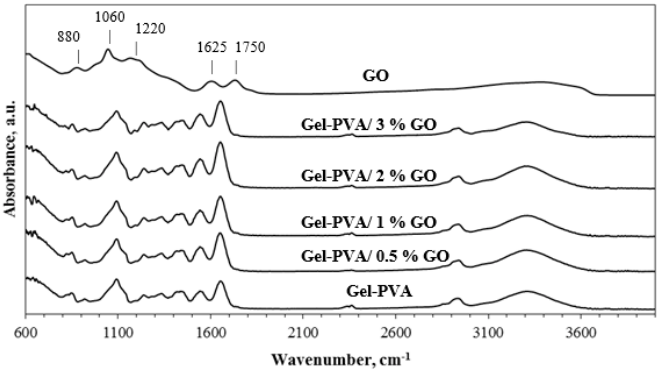

Fig. 2. FT-IR spectra of pure GO and Gel-PVA/GO scaffolds

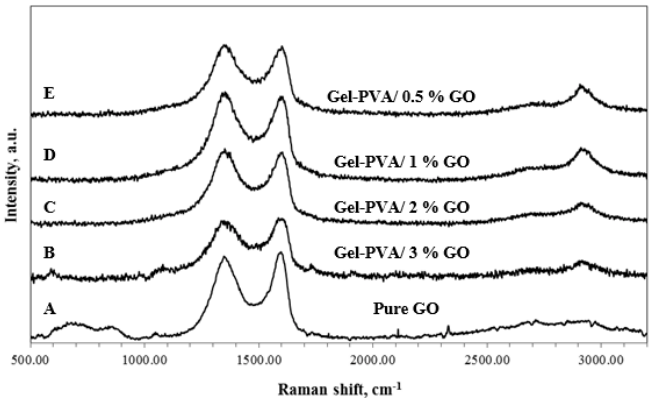

Fig. 3. Raman spectra of GO and Gel-PVA/GO composites and pure GO

stretching vibrations of C=O bond. The 1540 cm^{-1} absorption band specific for Amide II mode reflects the combination of N-H in plane bend together with C-N stretching vibration [30]. The 1200-1400 cm^{-1} region shows the complex Amide III mode defined by in-plane vibrations of the C-N and N-H of the amide bonds, or vibrations of the CH_2 groups of glycine [31].

In the case of pure PVA scaffold, all major peaks related to hydroxyl and methylene groups were detected. A broad and intense O-H absorption stretching band is observed between 3100-3500 cm^{-1}, indicating the intramolecular and intermolecular hydrogen bonding [32]. The two distinct absorption bands occurring at 2945 and 2920 cm^{-1} resulted from anti-symmetric and symmetric stretching bands of CH_2 groups respectively. The shoulder-like band found at 2850 cm^{-1} can be attributed to the C-H stretching vibration. The bands at 1435 cm^{-1} and 1335 cm^{-1} result from the CH_2 symmetric bending and wagging vibration respectively [33]. The most intense peak of the PVA spectrum is located at 1100 cm^{-1} arising from the C-O stretching vibration, while the shoulder can be observed at 1143 cm^{-1} which is known to be the crystallization-sensitive band of PVA, being taken as a measure of the crystallinity degree [33]. The final band of the pure PVA spectrum (860 cm^{-1}) is assigned to the C-C stretching vibration.

The spectrum of Gel-PVA blend presents all the characteristic signals of the two components but does not reveal new absorption bands or band shifts, indicating that there were no major changes of the functional groups induced by the interactions between PVA and gelatin.

The FT-IR spectrum of GO (fig. 2) confirmed the presence of different types of oxygen functionalities, the peaks at 1060, 1220 and 1750 cm^{-1} corresponding to C-O-C, C-OH and C=O stretching vibrations have been detected [34, 35]. The broad band between 3000-3700 cm^{-1} has been assigned to the O-H stretching vibrations of the hydroxyl groups present in the structure of GO together with possible OH groups of water molecules adsorbed on its surface [36]. Finally, the peaks at 880 and 1625 cm^{-1} reveal the aromatic C-H bending and C=C stretching vibrations of the sp^2 carbon skeletal network of graphite.

The presence of GO and chemical interactions between the Gel-PVA blend and GO could not be detected using FT-IR spectroscopy (fig. 2). A reason for this could be the low concentration of graphene oxide leading to inferior intensity absorption bands in comparison to the ones exhibited by the polymeric blend.

Raman spectrometry

Raman spectroscopy is a non-destructive technique that is widely used to obtain carbon-based materials structural information. It is also a valuable tool to investigate disorder and defects in molecular structure of these materials [37].

The spectrum associated with GO exhibits two main proeminent peaks associated with GO displayed (fig. 3. A), D and G bands. The D band located at 1353 cm^{-1} is attributed to a defect-induced breathing mode of sp^2 aromatic rings [38], while G band detected at 1595 cm^{-1} is characteristic for the graphitic layers and represents the in-plane stretching vibrations of sp^2 C-C bonds [39]. The very broad absorption band between 2500 and 3150 cm^{-1} arises from a two photon double resonance Raman process, known as the 2D band and is the overtone of the D band [37].

Besides the D and G bands, the Raman spectra of synthesized composite scaffolds present two more bands (fig. 3. B-E). The first one is a shoulder-like band emerging at 2720 cm^{-1} and represents the 2D band of GO. The absorption band found at 2910 cm^{-1} is mainly attributed to the stretching vibrations of C-H bonds of PVA backbone chain [40-42]. As the GO concentration is increased the CH_2 vibration band is more difficult to be detected as the signal gets covered by the one exhibited by the broad 2D band of GO.

The relative intensity ratio of both peaks (I_D/I_G) is an useful parameter for expressing the disorder degree of GO, revealing the structural changes induced by the physical interactions with the polymer matrix [39, 43, 44]. As seen in figure 4, the D/G intensity ratio for composite materials is slightly increased in comparison with pure GO. Such results could be generated by GO nanosheets bending and folding during the scaffolds fabrication process, while the higher intensity ratio obtained for the 3 wt.% GO scaffold suggests an increased structural disorder at high GO loadings [22]. The Raman spectra of synthesized biocomposites indicates GO is good dispersion in the polymer matrix and that there was minor damage to the

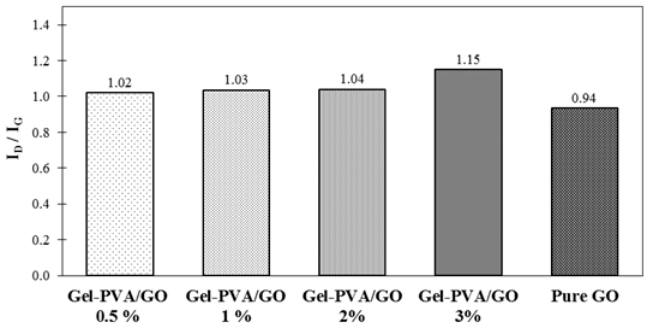

Fig. 4. D/G intensity ratios of GO and Gel-PVA/GO composites

GO nanosheets during fabrication process in terms of defects induced.

Scanning electron microscopy

The morphology of scaffolds is highly dependent on processing conditions like temperature, rate, time, and direction of freezing as well as on conditions of defrosting, both employed during the freeze-thawing process [45]. Figure 5 presents Gel-PVA scaffold micrographs, revealing the formation of various pore geometries and dimensions along cross-section area. In order to compare the morphology of synthesized scaffolds the middle region was selected as reference.

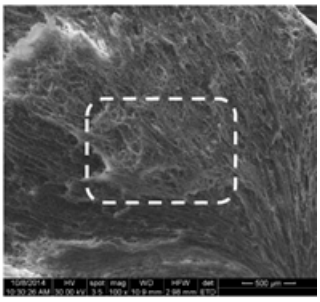

Fig. 5. Reference region on cross section area of Gel-PVA scaffold

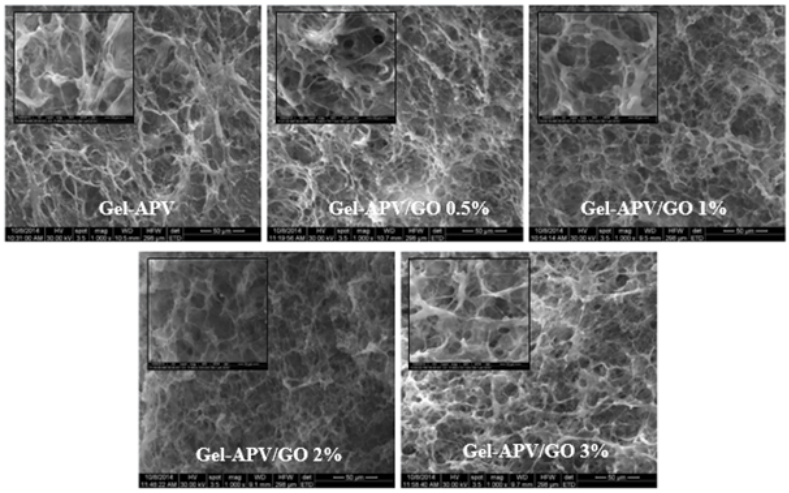

Fig. 6. SEM micrographs of Gel-PVA and Gel-PVA/GO composites

Figure 6 reveals that all synthesized scaffolds exhibit highly porous structures having a sponge-like aspect and irregular pore size distributions. The pore diameter of unloaded polymer matrix varies between 10 and 50μm and after the incorporation of GO only a slight decrease in pore size is registered.

The most significant morphology difference was exhibited by the composite presenting GO loading higher than 0.5 wt%. A reason for this behavior is the enhanced dispersion of GO within the polymer matrix ensuring strong and homogeneous intermolecular interactions.

A specific morphology was obtained for the 2 wt% GO containing scaffold which exhibited a regular pore size distribution with well interconnected pores and thin pore walls.

Swelling studies

Swelling capacity plays an important role in the absorption of body fluids and in the transfer of nutrients and metabolites to the cell [46, 47].

The swelling behavior of synthesized scaffolds (fig. 7) reveal a super-porous hydrogel character [48, 49]. Thus, materials present a rapid fluid uptake in the first minutes of immersion as a result of pore interconnectivity which act as a capillary system [49]. As shown in figure 7, all scaffolds reach equilibrium state in less than one hour and they absorb between 5 to 8 times their initial weights.

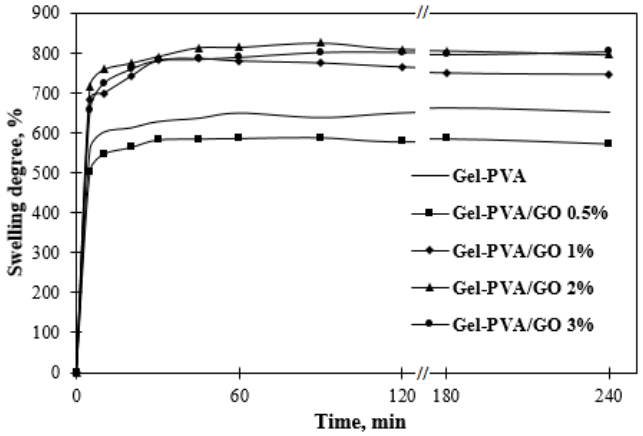

Fig. 7. Swelling capacity of synthesized scaffolds

These observation are in agreement with SEM results, which indicated an enhanced pore interconnectivity under the influence of GO, swelling degree presented an increased fluid uptake for scaffolds with GO concentrations higher than 1%. The reason behind this behavior is that GO facilitates formation of a network composed of macro- and micro- channels that ensures higher fluid infiltration. On the other hand, the lowest amount of GO added within the polymer matrix caused a lower fluid uptake due to a shrinkage in pore diameter and low pore interconnectivity, as shown by SEM.

Hydrolytic degradation behaviour

All biodegradable polymers contain hydrolysable bonds which makes them susceptible to chemical degradation via hydrolysis. The ideal biodegradation rate would be the same or slightly lower than the rate of cell

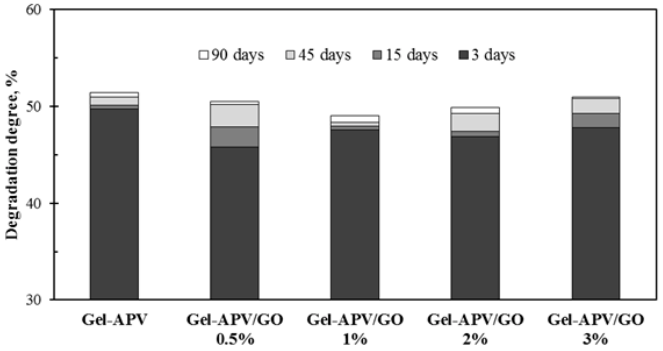

Fig. 8. Scaffold degradation degrees

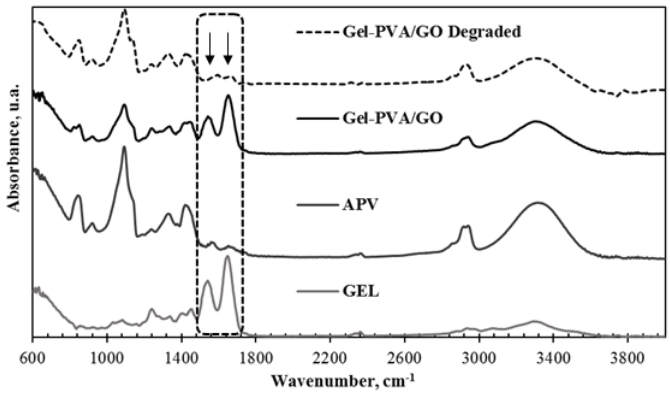

Fig. 9. FT-IR spectrogram of 0.5 wt.% Gel-PVA/GO scaffold after degradation

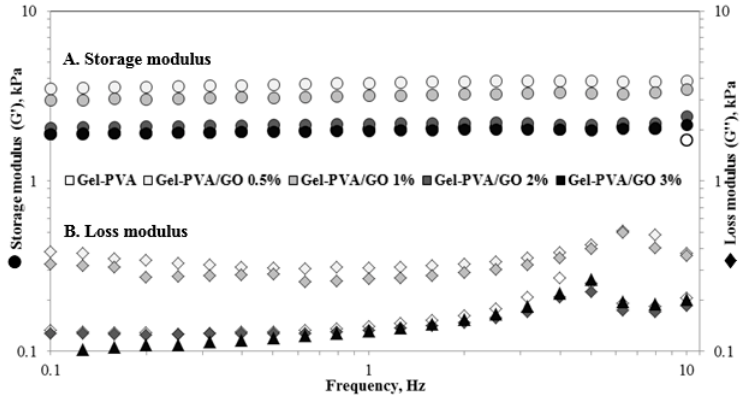

Fig. 10. Frequency influence on storage (G') and loss (G'') modulus of scaffolds

in-growth inside the scaffold in order to allow the new tissue to replace the polymer network [50].

For the Gel-PVA/GO scaffolds, the most rapid degradation stage occurred in the first 3 days (fig. 8). The GO-free scaffold exhibited the highest degradation degree in this stage, confirming that the addition of GO slightly reinforces the scaffolds by physical interactions. In the second stage, between 3 and up to 90 days only minor degradation (less than 5 wt.%) occurred for all scaffolds. Although the scaffold containing 0.5 wt.% GO exhibited the lowest degradation rate in the first 3 days, overall the 1 wt.% GO containing scaffold attained the least degradation degree. Generally, after 90 days, incorporation of GO didn't show a significant influence on the degradation rates of synthesized scaffolds.

In order to investigate the structural modifications occurred after hydrolytic degradation, FT-IR analysis was performed on degraded and non-degraded GO containing scaffolds and compared with gelatin and polyvinyl alcohol spectra.

By analyzing the FT-IR spectra (fig. 9) it was noticed that the hydrolytic degradation altered the composition of the materials. More specifically, the characteristic adsorption bands of gelatin were no longer detected in the composite spectrum registered after material degradation. In consequence, the weight loss is mainly attributed to gelatin migration occurring via solubilisation-diffusion mechanism in the absence of covalent crosslinking.

Scaffold rheology

The frequency sweep test revealed that the solid-like component, storage modulus G', shows almost no dependence with frequency (fig. 10. - A) indicating a good stability for all synthesized scaffolds on the entire frequency domain. The fact that the storage modulus is far much higher than the loss modulus (fig. 10 - B) indicates that the elastic response of the materials is stronger than the viscous response (G'>>G''). Thus, the scaffolds display a predominantly solid-like behavior suggesting that an elastic gel network has been formed [51]. These findings are in strong agreement with swelling results which revealed that the materials present a super-porous hydrogel character.

The highest storage modulus was achieved by the scaffold containing 0.5 wt.% GO, with a 90% increase as compared to the GO-free polymer matrix. This is also in agreement with swelling results which indicated a lower swelling capacity for 0.5 wt.% GO/Gel-PVA composites. Thus, if less water is absorbed by the scaffold there is less lubrication between polymer chains and the composite material remains rigid. Another explanation for this behaviour is that an efficient exfoliation and dispersion of GO sheets within the polymer up to 1 wt.%, while GO tends to form agglomerates and loses its efficiency as reinforcing agent, as the concentration increase to 2 and 3 wt.%, respectively.

Regarding the values obtained for the loss moduli (G''), there can be observed a high-amplitude noise recorded between 5 and 10 Hz (fig. 10. - B). This is the result of low adhesion forces at the interface between the sample and the metal plates which allowed the specimens to slide out at high frequencies. However, this is also a proof that the synthesized scaffolds are *strong gels*, having a higher tendency towards slipping rather than deforming under high-frequency shear stress.

The storage moduli of synthesized Gel-PVA/GO scaffolds range from 2 to 3.8 kPa. While these values represent the lower stiffness limit for tissues and cell-culture substrates, it does cover an important compliance range in soft tissue engineering [52].

Conclusions

The study confirms that porous 3D scaffolds based on gelatin - polyvinyl alcohol polymer matrix reinforced with graphene oxide could be successfully prepared by freeze-thawing combined with freeze-drying technique.

FT-IR spectra of synthesized materials did not reveal new absorption bands or band shifts, indicating that there were no covalent interactions established between the three components. While Raman spectra confirmed the

presence of GO inside the polymer matrix and the intensity ratios of D and G bands (I_D/I_G) suggested that the GO nanosheets present an increased structural disorder at high nanofiller concentrations.

The morphology of the scaffolds as shown by SEM micrographs exhibit highly porous structures with sponge-like aspect and irregular pore size distribution (10-50μm). GO incorporation facilitates pores interconnectivity. This results are in agreement with swelling studies which indicated an increased swelling degree for composite materials having GO concentrations higher than 0.5 wt.%.

Regarding the hydrolytic degradation experiments, results showed that all scaffolds suffered degradation between 45 and 50% in the first three days regardless of the GO content. The weight loss was mainly attributed to gelatin migration occurring through a solubilisation-diffusion mechanism in the absence of chemical crosslinking. Thus, the physical crosslinking is not sufficient in order to efficiently stabilize the gelatin inside the polymer matrix.

The rheological investigations revealed that the scaffolds display a solid-like behavior and indicates the formation of an elastic gel network. Moreover, it was found that the amount of 0.5 wt.% GO has the best reinforcing effect upon the polymer matrix, reaching an almost double storage modulus in comparison to the GO-free scaffold. This was also proved by swelling studies which indicated a low swelling degree for the 0.5 wt.% GO-containing scaffold. Thus, the incorporation of low GO amounts inside Gel-PVA polymer matrix can enhance the mechanical stability of the scaffolds.

Acknowledgements: The financial support was ensured by The Romanian National Authority for Scientific Research, Executive Agency for Higher Education, Research, Development and Innovation, project number PN-II-PCCA-14/2012. Celina Damian acknowledge funding by the Sectoral Operational Programme Human Resources Development 2007-2013 of the Ministry of European Funds through the Financial Agreement POSDRU/159/1.5/S/132397. The SEM analyses on samples were possible due to EU-funding grant POSCCE-A2-O2.2.1-2013-1/Axa prioritara 2, Project No. 638/12.03.2014, cod SMIS-CSNR 48652

References

1. O'BRIEN F.J., Materials Today, **14**, no.3, 2001, p. 88-95.
2. KARP J.M., LANGER R., Current Opinion in Biotechnology, **18**, no. 3, 2007, p. 454-459.
3. STEVENS M.M., Materials Today, **11**, no.5, 2008, p. 18-25.
4. CHAN B.P., LEONG K.W., Eur Spine J., **17**, no.4, 2008, p. 467-479.
5. MURPHY C.M., O'BRIEN F.J., LITTLE D.G., SCHINDELER A., European Cells and Materials, **26**, 2013, p. 120-132.
6. IMRE B., PUKÁNSZKY B., European Polymer Journal, **49**, no. 6, 2013, p. 1146-1150.
7. SALGADO A.J., COUTINHO O.P., REIS R.L., Macromol. Biosci., **4**, no. 8, 2004, p. 743-765.
8. YUSOP A.H., BAKIR A.A., SHAHAROM N.A., ABDUL KADIR M.R., HERMAWAN H., International Journal of Biomaterials, **2012**, 2012, 10 p. doi:10.1155/2012/641430.
9. DONG Z., LI Y., ZOU Q., Applied Surface Science, **255**, 2009, p. 6087-6091.
10. ULLM S., KRUGER A., TONDERA C., GEBAUER T.P., NEFFE A.T., LENDLEIN A., JUNG F., PIETZSCH J., Biomaterials, **35**, no. 37, December 2014, p. 9755-9766.
11. DU L., KHIARI Z., PIETRASIK Z., BETTI M., Poultry Science, **92**, 2013, p. 2463-2474.
12. DREESMANN L., AHLERS M., SCHLOSSHAUER B., Biomaterials, **28**, no. 36, December 2007, p. 5536-5543.
13. ROSE J.B., PACELLI S., EL HAJ A.J., DUA H.S., HOPKINSON A., WHITE L.J., ROSE F.R.A.J., Materials, **7**, 2014, p. 3106-3135.
14. OKAMOTO M., BAIJU J., Progress in Polymer Science, **38**, no. 10-11, Oct–Nov 2013, p. 1487-1503.
15. YE M., MOHANTY P., GHOSH G., Materials Science and Engineering: C, **42**, Sept. 2014, p. 289-294.
16. GEORGIEVA N., BRYASKOVA R., TZONEVA R., Materials Letters, **88**, Dec. 2012, p. 19-22.
17. GUAN Y., BIAN J., PENG. F., ZHANG X.M., SUN R.C., Carbohydrate Polymers, **101**, Jan 2014, p. 272-280.
18. PEPPAS N., Makromol. Chem., **176**, 1975, p. 3433.
19. AFSHARI M.J., SHEIKH N., AFARIDEH H., Radiation Physics and Chemistry, **113,** Aug. 2015, p 28-35.
20. LIU Y., GEEVER L.M., KENNEDY J.E., HIGGINBOTHAM C.L., CAHILL P.A., McGUINNESS G.B., J Mech Behav Biomed Mater., **3**, no.2, Feb. 2010, p. 203-209.
21. GEIM A.K., NOVOSELOV K.S., Nature Materials, **6**, 2007, p. 183-191.
22. IONITA M., PANDELE A.M., CRICA L., PILAN L., Composites Part B: Engineering, **59**, Mar. 2014, p. 133-139.
23. ROHINI R., KATTI P., BOSE S., Polymer, **70**, Jul. 2015, p. A17-A34.
24. DEPAN D., GIRASE B., SHAH J.S., MISRA R.D.K., Acta Biomaterialia, **7**, no. 9, Sept. 2011, p. 3432-3445.
25. DREYER D.R., PARK S., BIELAWSKI C.W., RUOFF R.S., Chem Soc Rev., **39**, no. 1, Jan 2010 p. 228-40.
26. ZHANG L., WANG Z., XU C., LI Y., GAO J., WANG W., LIU Y., Journal of Materials Chemistry, **21**, 2011, p. 10399-10406.
27. IONITA M., VASILE E., CRICA L.E., VOICU S.I., PANDELE A.M., DINESCU S., PREDOIU L., GALATEANU B., HERMENEAN A., COSTACHE M., Composites Part B: Engineering, **72**, Apr. 2015, p. 108-115.
28. HUMMERS JR. W.S., OFFEMAN R.E., Journal of American Chemical Society, **80**, no. 6, 1958, p. 1339–1339.
29. YAKIMETS I., WELLNER N., SMITH A.C., WILSON R.H., FARHAT I., MITCHELL J., Polymer, **46**, 2005, p. 12577–12585.
30. BARTH A. ZSCHERP C., Quarterly Reviews of Biophysics, **35**, no.4, 2002, p. 369–430.
31. SILVA G.G.D., SOBRAL P.J.A., CARVALHO R.A., BERGO P.V.A., MENDIETA-TABOADA O., HABITANTE A.M.Q.B., **16**, 2008, p. 276-285, DOI 10.1007/s10924-008-0112-9.
32. MANSUR H.S., COSTA H.S., Chemical Engineering Journal, **137**, 2008, p.72–83.
33. SHEHAP A.M., Egypt. J. Solids, **31**, no.1, 2008, p. 75-91.
34. DEPAN D., GIRASE B., SHAH J.S., MISRA R.D.K., Acta Biomaterialia, **7**, 2011, p. 3432–3445.
35. CHOI E.Y., HAN T.H., HONG J., KIM J.E., LEE S.H., KIM H.W., KIM S.O., J.Mater.Chem., **20**, 2010, p. 1907–1912. DOI: 10.1039/b919074k.
36. SHAHRIARY L., ATHAWALE A.A., International Journal of Renewable Energy and Environmental Engineering, **2**, no.1, 2014, p. 58-63.
37. SAHOO S., HATUI G., BHATTACHARYA P., DHIBAR S., DAS C.K., Graphene, **2**, 2013, p. 42-48.
38. FERRARI A.C., ROBERTSON J., Phys. Rev. B, **61**, 2000, p. 14095-14107.
39. SOBON G., SOTOR J., JAGIELLO J., KOZINSKI R. et al., Optics Express., **20**, no. 17, 2012, p. 19463-73.
40. PROSANOV I.Y., MATVIENKO A.A., Physics of the Solid State, **52**, no 10, 2010, p. 2203-2206.
41. DEEPAK K.L.N., SOMA V.R., DESAI N.R., Laser Pulses - Theory, Technology, and Applications, Prof. Igor Peshko (Ed.), ISBN: 978-953-51-0796-5, InTech, DOI: 10.5772/45854.
42. ZHANG M., KELLEHER E.J.R., TORRISI F., SUN Z., HASAN T., POPA D., WANG F., FERRARI A.C., POPOV S.V., TAYLOR J.R., **Optics Express, 20, no. 22, 2012,** p. 25077-25084.
43. SHIMODAIRA N., MASUI A., Journal of Applied Physics, **92**, 2002, p. 902-909.
44. XU J., GAO Q., ZHANG Y., TAN Y., TIAN W., ZHU L., JIANG L., Scientific Reports, **4**, 2014, p. 5545, doi:10.1038/srep05545.
45. DHANDAYUTHAPANI B., YOSHIDA Y., MAEKAWA T., KUMAR D.S. , International Journal of Polymer Science, **2011**, 2011, 19 p. doi:10.1155/2011/290602.

46. LI J., SUN H., SUN D., YAO Y., YAO F., YAO K., Carbohydrate Polymers, **85**, no. 4, Jul. 2011, p. 885-894, ISSN 0144-8617, http://dx.doi.org/10.1016/j.carbpol.2011.04.015.
47. PETER M., GANESH N., SELVAMURUGAN N., NAIR S.V., FURUIKE T., TAMURA H., RAJAKUMAR R., Carbohydrate Polymers, **80**, no. 3, May 2010, p. 687-694, ISSN 0144-8617, http://dx.doi.org/10.1016/j.carbpol.2009.11.050.
48. GANJI F., VASHEGHANI-FARAHANI S., VASHEGHANI-FARAHANI E., Iranian Polymer Journal, **19**, no. 5, 2010, p. 375-398.
49. TURAKHIYA J.M., SAVANI H.D., PATEL J.M., AKBARI B.V., PRAJAPATI N.G., SHAH V.S., Universal Journal of Pharmacy, **2**, no.1, 2013, p. 47-58.
50. ENGINEER C., PARIKH J., RAVAL A., Trends Biomater. Artif. Organs, **25**, no. 2, 2011, p. 79-85.
51. CHEN D.T.N., WEN Q., JANMEY P.A., CROCKER J.C., YODH A.G., Annu. Rev. Condens. Matter Phys., **1**, 2010, p. 301–322.
52. VANDERHOOFT J.L., ALCOUTLABI M., MAGDA J.J., PRESTWICH G.D., Macromol. Biosci., **9**, 2009, p. 20–28

Manuscript received: 9.12.2015